analytical chemistry

Article

pubs.acs.org/ac

Toward a Droplet-Based Single-Cell Radiometric Assay

Maria Elena Gallina,[†,×] Tae Jin Kim,[†,×] Mark Shelor,[‡] Jaime Vasquez,[§] Amy Mongersun,[∥] Minkyu Kim,[⊥] Sindy K. Y. Tang,[⊥] Paul Abbyad,[∥] and Guillem Pratx*[,†]

[†]Division of Medical Physics, Department of Radiation Oncology, Stanford University, 300 Pasteur Drive, Palo Alto, California 94305, United States

[‡]University of California-Merced, Department of Bioengineering, 5200 North Lake Road, Merced, California 95343, United States

[§]University of California-San Francisco, School of Pharmacy, 600 16th Street, San Francisco, California, 94158, United States

[∥]Department of Chemistry and Biochemistry, Santa Clara University, Daly Science 123500 El Camino Real, Santa Clara, California 95053, United States

[⊥]Department of Mechanical Engineering, Stanford University, 418 Panama Mall, Stanford, California 94305, United States

Supporting Information

ABSTRACT: Radiotracers are widely used to track molecular processes, both *in vitro* and *in vivo*, with high sensitivity and specificity. However, most radionuclide detection methods have spatial resolution inadequate for single-cell analysis. A few existing methods can extract single-cell information from radioactive decays, but the stochastic nature of the process precludes high-throughput measurement (and sorting) of single cells. In this work, we introduce a new concept for translating radioactive decays occurring stochastically within radiolabeled single-cells into an integrated, long-lasting fluorescence signal. Single cells are encapsulated in radiofluorogenic droplets containing molecular probes sensitive to byproducts of ionizing radiation (primarily reactive oxygen species, or ROS). Different probes were examined in bulk solutions, and dihydrorhodamine 123 (DHRh 123) was selected as the lead candidate due to its sensitivity and reproducibility. Fluorescence intensity of DHRh 123 in bulk increased at a rate of 54% per Gy of X-ray radiation and 15% per MBq/ml of 2-deoxy-2-[^{18}F]-fluoro-D-glucose ([^{18}F]FDG). Fluorescence imaging of microfluidic droplets showed the same linear response, but droplets were less sensitive overall than the bulk ROS sensor (detection limit of 3 Gy per droplet). Finally, droplets encapsulating radiolabeled cancer cells allowed, for the first time, the detection of [^{18}F]FDG radiotracer uptake in single cells through fluorescence activation. With further improvements, we expect this technology to enable quantitative measurement and selective sorting of single cells based on the uptake of radiolabeled small molecules.

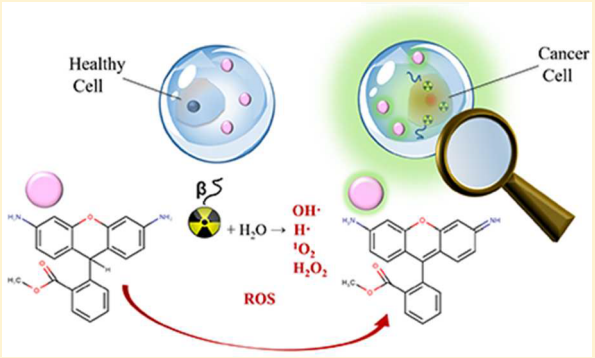

Radiotracers are unique functional probes of biochemical processes both *in vivo* and *in vitro*. In comparison to antibodies and oligonucleotides, which target specific phenotypes through the selective recognition of a specific biomarker, radioactive probes can measure the real-time metabolic activity of transporters and downstream enzymes and, therefore, probe the activity of well-defined cellular pathways. This functional type of assay has the capability of revealing biological mechanisms with molecular specificity, enabling a rich array of clinical and preclinical applications.[1] Notably, radionuclide imaging techniques such as positron emission tomography (PET)[2−5] play an important role in hospitals and in research laboratories, where they are used to diagnose, stage, and monitor the treatment of a variety of diseases. Conventional methods for radionuclide detection also include liquid scintillation counting, gamma counting, and autoradiography. Furthermore, radionuclide substitution is suitable to investigate the biochemical activity of small molecules, because it requires minimal modification of their chemical structure. As a consequence, radiotracers are commonly used in the pharmaceutical industry to support the selection of new drug candidates and for regulatory approval. With respect to this, a novel microfluidic radioassay was recently proposed to acquire detailed cellular pharmacokinetics using a positron camera.[6] Despite their utility and sensitivity, a general downside of conventional radionuclide methods is their poor spatial resolution, which prevents their use at the single-cell level. As a matter of fact, most single-cell studies are currently based on fluorescence methods, where the use of bulky, organic fluorophores is prone to affect biochemical properties.

Accomplishing single-cell resolution has become a crucial goal ever since cellular heterogeneity was acknowledged as one of the greatest challenges of cancer therapeutics.[7−9] In this

Received: February 2, 2017
Accepted: May 31, 2017
Published: May 31, 2017

DOI: 10.1021/acs.analchem.7b00414
Anal. Chem. 2017, 89, 6472−6481

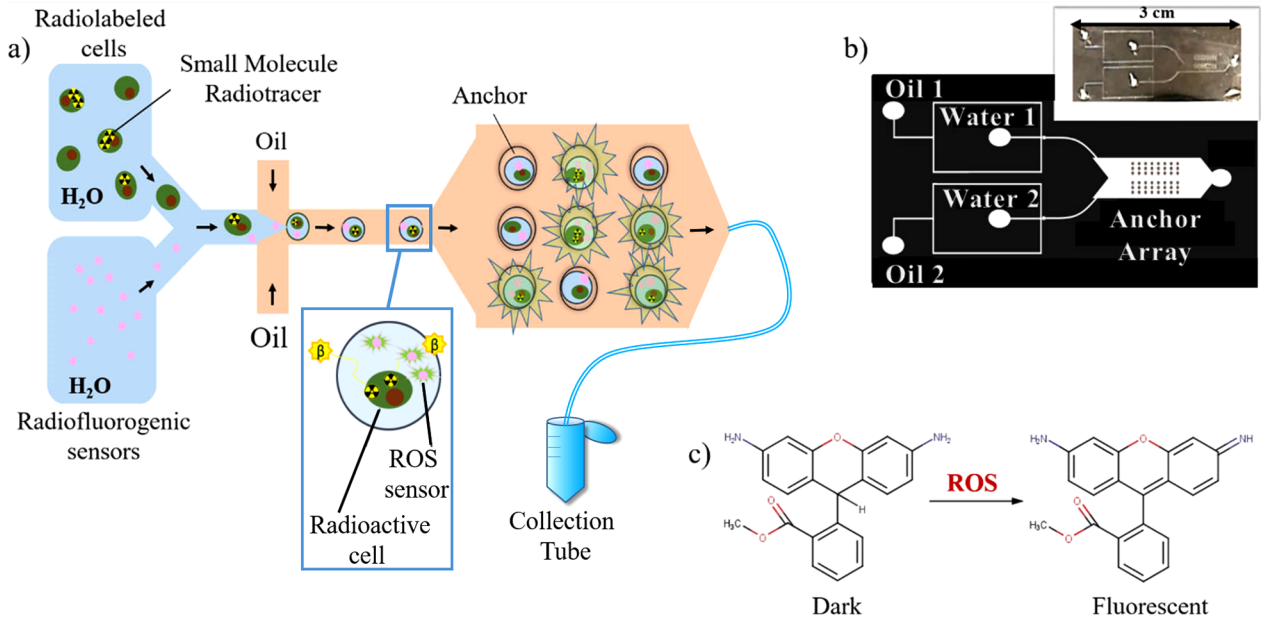

Figure 1. Overview of the experimental approach. (a) Workflow of the radiofluorogenic droplet assay: radiolabeled single cells suspended in PBS are mixed with radiofluorogenic sensors immediately before entering the flow focusing channel. Once the aqueous mixture forms into droplets, they are anchored to an array of microwells. Droplets that are not trapped by the anchors exit from the chip through an outlet tube and are collected in an Eppendorf tube for further testing. The actual chip is equipped with two flow focusing nozzles but only a single one is shown in this drawing. (b) Microfluidic channel design, showing the two parallel flow focusing nozzles, for the optional generation of two populations of droplets and the imaging chamber with its anchoring array. Each of the two flow focusing nozzles has a dedicated oil inlet (indicated as Oil 1 and Oil 2, respectively) and a dedicated inlet for the water phase (indicated as Water 1 and Water 2). In addition, the radiofluorogenic sensor can be mixed with the cell suspension directly at the water inlet by punching two input holes through the PDMS (diameter = 1.0 mm) into one of the two water inlets. The microwells are 25 μm deep. Inset: picture of device printed in PDMS. (c) Conversion of DHRh 123 to rhodamine 123 followed by reaction with ROS.

context, flow cytometry, a fundamental tool in the diagnosis of cancers such as leukemia and lymphoma, is used for determining cell differentiation by genotypic and phenotypic analysis of cell suspensions extracted from blood.[10] Despite the increased level of attention devoted to this topic, systematic investigations of cellular diversity using radiotracers are not available yet, prompting the need for novel, high-throughput methodologies.[11,12] Performing radionuclide detection in single cells would have many applications, ranging from basic research to drug development studies and clinical diagnostics. For example, single-cell radionuclide detection could complement flow cytometry by identification and sorting of cells characterized by aberrant metabolism, a common property of cancer cells. Our lab has recently developed a new technique known as radioluminescence microscopy (RLM),[13,14] to measure the amount of radiotracers in single cells. RLM detects beta particles emanating from individual cells placed in direct contact with an inorganic scintillator substrate.[15] Scintillation events are detected, processed, and numerically combined to yield an image of radionuclide distribution in cells. Fluorescence and bioluminescence microscopy can also be performed in conjunction to RLM for multimodal imaging.[16] Several studies were performed using RLM to study heterogeneity at the single-cell level, revealing unexpected patterns in the pharmacokinetics of commonly used radiotracers. 2-Deoxy-2-[^{18}F]-fluoro-D-glucose ([^{18}F]FDG), a glucose analogue used as the principal clinical tool in cancer diagnostics via PET imaging, was used as an ideal tool for proof-of-concept studies. In RLM studies, the uptake of [^{18}F]FDG exhibited considerable heterogeneity even within the same cancer cell line.[13,15,17] This result is quite significant if we consider that preferential uptake of [^{18}F]FDG is interpreted as a distinctive property of cancer tissues.[18,19] In another study, the analysis of 3′-deoxy-3′-[^{18}F]fluorothymidine ([^{18}F]FLT) uptake in single cells revealed a bimodal distribution, indicative of the fraction of actively dividing cells present in the total population.[20] In addition, the uptake of radiolabeled anticancer drugs can be interrogated with single-cell resolution, and investigations on rituximab pointed out extremely inhomogeneous levels of uptake in tissues and single cells.[14]

Although RLM has high sensitivity and spatial resolution, its use remains limited because it can analyze only a small number of cells at a time and it cannot easily sort the measured cells. The reason for the limited cell throughput is fundamentally linked to the physics of radioactive decay. Radioactive decay is a stochastic process, meaning that decay events are spontaneous rather than stimulated. Therefore, any cell of interest must be imaged continuously over a period of time long enough to detect a statistically robust number of radioactive events. This contrasts with fluorescence methods, where the fluorescent emission can be triggered on demand by illuminating the cell with a suitable wavelength. These characteristics make radionuclide detection at the microscopic level extremely difficult, and current methods require long acquisitions in sensitive, low-light settings to address this issue. As an example, RLM requires about 20 min to achieve a satisfactory signal-to-noise ratio for measuring less than 50 cells. These constrains result in low throughput and make it difficult to implement this approach for cell sorting, precluding any large-scale application.

To enable radionuclide measurements in cells in a high-throughput manner, we propose the conversion of random radioactive decays emitted from single cells into a permanent,

DOI: 10.1021/acs.analchem.7b00414
Anal. Chem. 2017, 89, 6472−6481

integrated optical signal. In our approach, this translation is realized through the use of radiofluorogenic sensors,[21−23] i.e., molecular precursors which convert irreversibly to fluorophores in response to ionizing radiation. The activation mechanism of these probes is mediated by the presence of reactive oxygen species (ROS), which are produced as a consequence of water radiolysis by ionizing beta particles (electrons or positrons). ROS can react instantaneously with radiofluorogenic probes, generating a fluorescence signal proportional to the radioactivity level. This approach is designed to detect the presence and the amount of radiotracers by fluorescence measurements, which can be performed with high-throughput techniques and could be the basis for cell-sorting applications. In addition, in contrast to other types of optical sensors for ionizing radiation,[24−26] ROS probes are commercially available, biocompatible, and water-soluble.[9,27,28,40]

Previously, a droplet-based scintillation platform was demonstrated[29] to increase cell throughput, but because its readout was still based on detecting individual decay events, no more than a few hundred cells could be measured in a single run. In the present design, single cells are coencapsulated with a ROS sensor into individual water-in-oil droplets (Figure 1a) using a microfluidic platform (Figure 1b). Here, fluorescence activation is triggered independently in each droplet by the positrons emitted from encapsulated single cells. This droplet compartmentalization presents many advantages: first, the ROS sensor is dissolved in droplets instead of being incorporated inside of the cell. In this configuration, the amount of sensor per cell is not influenced by the variability of its cellular uptake. Additionally, since most of these species are short-lived (their lifetime is in the order of nanoseconds), they remain confined inside the cells and cannot activate the sensor dissolved in the droplets. Therefore, nonspecific activation of the sensor by intracellular ROS generated by oxidative stress[30−32] can be neglected. These properties make the present technique particularly suitable to study heterogeneous pools of cells. Second, the influence of cell efflux is removed, as any effluxed radiotracer remains trapped in the droplet. Finally, microfluidic droplets are compatible with previously developed fluorescence-based platforms for high-throughput reading and sorting.[33,34]

The proposed technique is designed for the purpose of eventually sorting live cells on the basis of their biochemical activity along specific pathways. This method is conceptually similar to standard fluorescence-activated cell sorting (FACS), but instead of detecting specific cell-surface biomarkers, cells will be isolated on the basis of a functional assay, which provides real-time information on the activity of a given pathway (for instance, glycolysis or nucleotide salvage) or on the binding affinity of a radiolabeled small molecule to a cellular target. Since a given pathway may involve the cooperation of multiple enzymes, the proposed method provides a different readout than conventional flow cytometry. In this context, the isolation of live cells with abnormal pathway activity or drug binding affinity paves the way for improving the characterization of cancer subtypes and for studying the pharmacokinetics of targeted therapeutics at the single-cell level. This technique is also expected to find applications in small-molecule studies for drug development and for the formulation of new radiotracers.

The aim of this work is to establish the feasibility of the proposed platform through numerical simulations and experiments. First, we investigated the response of bulk solutions of different ROS sensors to X-ray and [^{18}F]FDG exposure. Dihydrorhodamine 123 (DHRh 123, Figure 1c) was identified among several candidates as a suitable radiofluorogenic probe for the detection of radiotracers and optimal working conditions were established. Then, the radiation dose response of DHRh 123 was tested in microfluidic droplets by fluorescence microscopy imaging. Possible experimental limitations such as cross-talk events between adjacent droplets were investigated and the feasibility of the proposed assay was verified. Finally, a proof-of-concept experiment was performed and we observed, for the first time, [^{18}F]FDG uptake in single cancer cells by fluorescence activation of microdroplets. These promising results provide a useful framework for designing the next-generation assay. We anticipate that, with further developments, this platform will constitute a high-throughput method for studying the distribution of a wide range of molecular imaging tracers in single cells using fluorescence detection.

MATERIALS AND METHODS

FDG Preparation. [^{18}F]FDG was prepared through nucleophilic ^{18}F-fluorination and hydrolysis of mannose triflate by the Stanford Cyclotron Radiochemistry Facility. ^{18}F was made in a GE PETtrace cyclotron and the production was performed via cassette-based automated synthetic module (FASTlab, GE Healthcare). Quality control tests were performed according to USP823. The radiotracer was used within 8 h after production due to its short halftime ($\tau_{1/2}$ = 1.8 h). Radioactivity was measured with a dose calibrator (Atomlab 400, Biodex) prior to each experiment.

ROS Sensor Selection. Various ROS sensors were evaluated to identify the one most suitable for this radiofluorogenic assay. DHRh 123 was purchased from Santa Cruz Biotechnologies. Singlet Oxygen Sensor Green (SOSG), Amplex Red Hydrogen Peroxide/Peroxidase Assay Kit, Aminophenyl Fluorescein, and Alexa 594 were purchased from Thermo Fisher Scientific, Inc. Coumarin-3-carboxylic (C3C) acid and 2′,7′-dichlorofluorescin diacetate (DCF-DA) were obtained from Sigma-Aldrich. ROS Star 550 was purchased from LI-COR Biosciences. PBS solutions of each sensor were dispensed in 96-well plates in four aliquots, each with a volume of 100 μL. Samples were irradiated with an X-RAD 320 X-ray irradiator (Precision X-ray) with a source-surface distance of 45 cm and a dose output set to 504.40 cGy/min (320 kVp, 12.5 mA and 2 mm thick aluminum filter).

Droplet Generation and Trapping. A microfluidic chip capable of generating and anchoring droplets for imaging was designed. The first section of the chip consists of two parallel microfluidic droplet generators (Figure 1b), used to produce two different groups of droplets simultaneously. For instance, one group of droplets may contain a radiotracer and the other group could serve as a control. As the droplets travel downstream, they merge into the second section of the chip, which consists of a single imaging chamber with an array of droplet anchors. The imaging chamber is useful to hold a small number of droplets in place and measure their fluorescence as it increases over time. Most droplets are not trapped and are collected at the outlet of the chip.

Polydimethylsiloxane (PDMS) microfluidic chips with channel depth modulations were fabricated using dry-film photoresist soft lithography technique described by Stephan et al.[35] Prior to bonding the PDMS microchannel to the glass substrate, inlet and outlet holes were punctured using a 1 mm diameter disposable biopsy punch (Claflin Medical Equipment

DOI: 10.1021/acs.analchem.7b00414
Anal. Chem. 2017, 89, 6472−6481

Co.). The PDMS chips were then bonded to a 25 mm × 75 mm × 1.0 mm precleaned glass microscope slides (Fisherbrand) with a corona discharger (Electro-technic Products). After 24 h of incubation in a vacuum chamber, the surface was made hydrophobic by flowing in Novec 1720 Electronic grade Coating (3M) through the microchannel and blow-drying with pressurized nitrogen gas. To minimize droplet shrinkage from dehydration, the microfluidic chip was saturated with water vapor prior to the experiment and sealed in a plastic bag with moist towels during experiments.

To generate droplets, HFE 7500 perfluorinated oil (3M) containing 2% w/w of 008-fluorosurfactant (RAN Biotechnologies) was used as the continuous phase, and DHRh 123 diluted in PBS was used as the dispersion phase. This formulation was chosen to minimize partitioning of rhodamine 123 (and most likely of DHRh 123) to the oil phase and to prevent droplets from coalescing. Syringe pumps (New Era Pump Systems, Inc.) drove the fluids at flow rates of 4 μL/min and 1 μL/min for the continuous phase and dispersion phase, respectively. The chip was equipped with flow focusing nozzles[36] to produce droplets (Figure 1b). Two different flow-focusing nozzles were used to allow the production of two distinct populations of droplets. These droplets flowed into an imaging chamber containing an anchor array consisting of microfabricated circular wells in the top of the channel.[37] Each anchor has a depth of 25 μm, a diameter of either 100 or 150 μm, and a center-to-center spacing of 150 and 170 μm apart, respectively. In this configuration, droplets were "pancake" shaped rather than spherical, squeezed between the top and bottom surfaces of the channel. The reduction in surface energy maintained the droplets in place despite the external flow of oil, forming an array. Droplets remained anchored to the imaging chamber for oil flow rates under 50 μL/min and they were removed by increasing the flow rate above 90 μL/min, allowing a fresh batch of droplets to be loaded into the anchors for subsequent imaging. For single-cell experiments, imaging of a large number of droplets was achieved by collecting the droplets in an Eppendorf tube located downstream of the anchor array. Novec 1720 (3M) was flowed in the plastic tubing prior to use as it helped prevent the droplets from coalescing. Droplets were then gently pipetted between two coverslips (Microscope Cover Glass, Fisher Scientific) for further imaging. This procedure allowed us to generate more uniform droplets than those anchored on the imaging chamber. This is because the anchor array trapped the first droplets made by the generator, and due to transient fluctuations in flow rate in the early time points, these droplets were more heterogeneous. Droplets made at later time points were more uniform and could be collected in larger quantities.

Cell Culture and Radiolabeling. Human breast adenocarcinoma cells (MDA-MB-231/Luc) cells were cultured at 37 °C and 5% CO_2 in DMEM medium supplemented with 10% fetal bovine serum and 1% penicillin-streptomycin (Thermo Fisher Scientific, Inc.). For radiolabeling, cells were incubated in [^{18}F]FDG (37 MBq/mL) dissolved in glucose-free DMEM for 60 min. After washing three times with PBS, cells were incubated for 5 min in Trypsin-EDTA 0.05% (Gibco, Thermo Fisher Scientific, Inc.), centrifuged, and resuspended in PBS with 16% OptiPrep density gradient medium (Sigma-Aldrich) at an approximate concentration of 1×10^6 cells/mL.

Fluorescence Detection and Image Analysis. Fluorescence spectra of bulk solutions were recorded using a SpectraMax M2 plate reader (Molecular Devices). Each data point is the average of at least three measurements. Fluorescence microscopy images were captured using two inverted fluorescence microscopes: an EVOS FL (Life Technologies) was used for studying the response of radiofluorogenic droplet to X-ray irradiation and [^{18}F]FDG solution, and a Leica DMi8 (Leica Microsystems, Germany) was used for the single-cell experiments. The EVOS FL was equipped with DAPI, GFP, and Texas Red dichroic filter sets, a Plan Fluorite 4× objective lens (NA = 0.13), and a 16-bit monochrome CCD camera (ICX445, Sony). The Leica DMi8 was equipped with a FITC dichroic set, a HC PL Fluotar 10× objective lens (NA = 0.32), and an 8-bit monochrome CCD camera (DFC3000 G, Leica). Fluorescence images were analyzed using ImageJ and the difference between the mean intensities of ROS sensor droplets and the image background was computed. The region of interest was drawn around each individual droplet manually, and the average fluorescence intensity was calculated on the entire droplet, including any cell present inside.

Monte Carlo Simulation. GEANT4 Monte Carlo simulations (GAMOS) were performed to estimate the cumulative ROS concentration as a function of droplet size and the nonspecific activation of radiofluorogenic droplets due to adjacent droplets containing radioactive cells. The cumulative ROS concentration was defined as the ratio between the total number of ROS generated in one droplet over time and the droplet volume. While the lifetime of ROS is generally very short (typically in the nanoseconds), the conversion of the sensor to a fluorescent product is irreversible, therefore the concentration of activated fluorophores is proportional to the cumulative ROS concentration. In the simulation, a single cell was modeled as a water sphere (diameter, 10 μm) containing a uniform amount of ^{18}F (10 Bq/cell), and it was placed at the center of a larger water droplet (with diameter ranging from 20 to 200 μm). The radioactive decay of ^{18}F was simulated over a period of 4 h, which corresponds to approximately twice its half-life; the energy deposited by ionizing particles in the droplet was scored and converted to cumulative ROS concentration on the basis of radiolytic yields.[38]

To estimate cross-contamination, we simulated two adjacent droplets with diameters of 85 μm, one empty and one containing a single radioactive cell. The center-to-center distance between the droplets was varied from 85 to 250 μm, and the amount of energy deposited in the empty droplet after 4 h was measured.

Safety Considerations. Radioactive compounds, such as [^{18}F]FDG, pose significant health risks. Institutional protocols should be followed for the handling and disposal of all radioactive materials.

RESULTS AND DISCUSSION

Experimental Concept and Monte Carlo Simulation. In this work, the uptake of [^{18}F]FDG by single cells was analyzed by imaging the fluorescence activation of droplets containing a known number of cells. The typical experiment workflow is shown in Figure 1a: following incubation with radiotracers, human breast cancer cells (MDA-MB-231) were suspended in PBS and injected into a microfluidic chip. The cell suspension was mixed with a solution of ROS sensors (DHRh123, 400 μM) traveling at the same flow rate in the microfluidic channel immediately before the formation of droplets. The schematic of the microfluidic chip used in this study is shown in Figure 1b. The chip was equipped with two

DOI: 10.1021/acs.analchem.7b00414
Anal. Chem. 2017, 89, 6472−6481

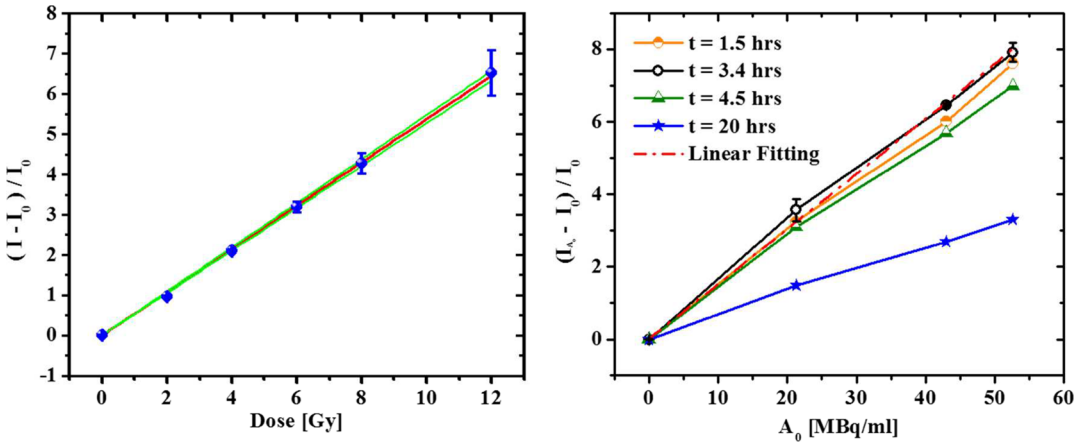

Figure 2. (a) Linear relationship between relative fluorescence intensity (525 nm) of DHRh 123 (50 μM in PBS) and X-ray radiation dose. The blue dots represent experimental data, the red line shows the linear regression curve ($\Delta I/I_0 = \Phi$Dose; Φ = 0.538 ($\pm$0.004) Gy^{1-}, R^2 = 0.9997), and the green lines are the 95% confidence bands. Standard deviations are reported (N = 3). (b) Graph of relative fluorescence intensity (525 nm) in bulk DHRh 123 (200 uM) solutions as a function of [^{18}F]FDG concentration at different times after adding the radiotracer with the sensor. The response at 3.4 h was analyzed by linear regression (red dashed-dotted line; $R^2 > 0.998$; $\Phi_{max}{}' = 1.5$ ($\pm$0.1) 10^{-1} mL/Bq). Standard deviations at 3.4 h are reported (N = 3).

Table 1. Physical and Chemical Properties of Investigated ROS Sensors[a]

sensor	λ_{ex} [nm]	λ_{em} [nm]	concn [μM]	detected ROS	Φ [Gy^{-1}]	Φ_{4h} [Gy^{-1}]	$\Delta\Phi\%_{4h}$	cell permeable
C3C	290	460	350	$HO^{\bullet}$	0.297	0.211	29	N
DHRh 123	500	530	200	H_2O_2, $ONOO^-$, NO	0.538	0.307	43	Y
SOSG	500	525	10	$^1O_2$	0.314	0.300	4.4	N
AMPLEX RED[b]	570	585	100	H_2O_2[b]	1.55	0.697[c]	55[c]	N
DCFH-DA	495	525	100	H_2O_2, $HO^{\bullet}$, $ROO^{\bullet}$	0.12	0.03	74	Y
APF	485	515	10	$HO^{\bullet}$,ClO^-, $ONOO^-$	1.47	0.23	84	Y
ROS-Star 550	546	561	200	$HO^{\bullet}$, $O_2^{\bullet-}$	0.12			Y

[a]Φ, sensor sensitivity; Φ_{4h}, sensitivity after 4 h; $\Delta\Phi\%_{4h}$, relative loss of sensitivity, i.e., instability. Linear regressions used to compute these data are reported in Figure S3. C3C, coumarin-3-carboxylic acid; DHRh 123, dihydrorhodamine 123; SOSG, singlet oxygen sensor green; DCFH-DA, 2′,7′-dichlorofluorescin diacetate; APF, aminophenyl fluorescein. [b]Interaction mediated by horseradish peroxidase (HRP). [c]Φ variation after 2 h only.

identical droplet generators to produce two distinct droplet populations. We used this feature of the chip to include a control group in some of the experiments. In addition, each of the two droplet generators was designed to allow two different solutions to be mixed right at the inlet, before the formation of droplets. We used this feature to mix the suspension of radioactive cells with the sensor solution, thus preventing the sensor from being activated before the droplet is formed. Downstream, droplets from both generators flowed directly into the imaging channel, which consisted of an array of microfabricated round wells used to anchors droplets for longitudinal imaging,[37] and then into a collection tube for further testing. Depending on the specific requirement of the experiments, either droplets trapped in the anchor array or those in the collection tube were imaged. Dosimetry and cross-talk studies were performed on droplets anchored to the imaging chip, since these droplets were kept in place by the anchors. In contrast, studies involving cell encapsulation were performed by injecting the droplets between two coverslips to obtain higher statistics.

The design of the assay reported here was optimized by simulating the physics of radiation transport inside a suspension of droplets using the Monte Carlo method. The goal of these simulations was 2-fold. First, we wanted to determine how the concentration of ROS in the droplet and the resulting fluorescent signal would vary as a function of droplet diameter. Second, we wanted to quantify to what extent a given droplet may receive an unwanted radiation dose from adjacent droplets.

In the first simulation study, the total energy deposited in the droplet was estimated as a function of droplet size and was compared to the radiolytic yields of two different ROS, hydroxyl radical ($^{\bullet}$OH; 2.75 molecule per 100 eV) and hydrogen peroxide (H_2O_2; 0.7 molecules per 100 eV).[38] These simulations showed that the cumulative concentration of these two ROS decreased as the droplet diameter increased (Figure S1a). Since droplet diameters ranged between 80 and 100 μm, the cumulative concentration of $^{\bullet}$OH radicals was expected to be between 100 and 200 nM.

In the second study, the probability that a beta ray coming from one droplet deposits its energy into another (radiation contamination) was investigated considering the case where the droplets are collected and stored tightly packed in an Eppendorf tube. Simulation results show that when two droplets touch each other, one may contaminate the other by ~11% of the total signal. Furthermore, considering droplets tightly packed in 3D, a given droplet may be closely surrounded by 12 others. Given the average occupancy of 0.32 cells per droplet in our configuration (diameter $\approx$ 85 μm, cell concentration $\approx 1 \times 10^6$ cells/mL), the potential radiation contamination was estimated to be at most ~42%. Because of the constant motion of droplets in solution, we expected the contamination to result in a baseline signal increase rather than in a fixed pattern.

DOI: 10.1021/acs.analchem.7b00414
Anal. Chem. 2017, 89, 6472−6481

Bulk Characterization and Selection of Radiofluorogenic Probes. A highly efficient ROS sensor is required to achieve high sensitivity with this assay; in this work, comparative tests were performed among seven candidates that satisfied the following requirements: commercial availability, water solubility and compatibility with cellular applications.[27,39] The sensors were dissolved in PBS, dispensed in a 96-well plate array, and exposed to increasing X-ray doses. In all cases, the fluorescence intensity increased linearly with increasing doses of X-ray radiation (Figure 2a and Figure S2). For comparison purposes, a sensitive sensor is defined as one that generates a large increase in fluorescence intensity for a given dose of X-ray radiation. In this context, sensitivity is mathematically represented by the slope Φ [units, Gy^{-1}] of the relative fluorescence intensity as a function of the radiation dose D:

$$\frac{I - I_0}{I_0} = \Phi D \tag{1}$$

where I_0 and I are the fluorescence intensities of nonirradiated and irradiated solutions, respectively. The sensitivity Φ was measured for the various investigated sensors (Table 1). Fluorescent intensity variations were also monitored at different times after X-ray exposure to monitor the occurrence of nonspecific fluorescence activation. The extent of this undesired phenomenon was quantified by defining instability as the relative change of sensitivity ($\Delta\Phi$%) within a defined time frame τ, in the absence of ionizing radiation:

$$\Delta\Phi\% = \frac{\Phi(t = 0) - \Phi(t = \tau)}{\Phi(t = 0)} \times 100\% \tag{2}$$

Stability measurements indicate that more sensitive sensors generally display higher levels of nonspecific fluorescence activation (Table 1).

Following this comparative analysis, three sensors were identified for their advantageous sensitivity and stability values: SOSG, C3C, and DHRh 123 (Table 1). However, SOSG was eliminated as a potential candidate because its high sensitivity could not be reliably reproduced in later experiments, likely due to the variability in the purity of commercial products. The second candidate, C3C, a well-known compound used in liquid radiation dosimetry,[40] was also rejected on account of its suboptimal spectral properties ($\lambda_{max.exc.}$ = 290 nm/$\lambda_{max.em.}$ = 460 nm) for conventional fluorescence microscopy. By elimination, DHRh 123 was chosen as the most promising commercial sensor; henceforth, its dosimetry performance was investigated in greater detail. By varying the concentration of the sensor, we observed that higher sensitivity could be achieved, but unfortunately, at these concentrations, the sensor also presented greater instability (Figure S3a). Therefore, the working concentration was set at an intermediate value, namely, 200 μM (Figure S3a).

Once the response of DHRh 123 to X-ray exposure was fully characterized, its response to beta-emitting radiotracers was investigated. Fluorescence activation by radioactive decay of [^{18}F]FDG was tested in bulk solutions at different time points and radioactivity concentrations. In the range of investigation (0−52 MBq/mL), the relative fluorescence intensity increased linearly with the radioactivity concentration (Figure 2b), and it was modeled according to

$$\frac{(I - I_0)}{I_0} = \Phi'[A_0] \tag{3}$$

where Φ' is the sensitivity of DHRh 123 to radioactive decays from [^{18}F]FDG, and $[A_0]$ is the initial radioactivity concentration. The relative fluorescence intensity reached its peak 3.4 h after mixing with [^{18}F]FDG, which corresponds to nearly two half-lives of ^{18}F. The maximum sensitivity was then quantified by linear regression at t = 3.4 h and found to be Φ_{max}' = 0.15 (±0.01) mL/MBq. This value, instead of reaching a plateau, decreased at later times. This phenomenon is attributed to the cumulative production of rhodamine 123 by slow, side reactions, which ultimately caused appreciable fluorescence activation in nonradioactive, reference solutions. Interestingly, the absolute intensity difference $(I - I_0)$ between positive (radioactive) and control samples remained constant over time, indicating that side reactions occur at the same rate.

The experimental evaluation of the sensor sensitivity was used to estimate the relative signal obtainable in radiometric cellular assays. In human cells, the average uptake of [^{18}F]FDG is about 5 Bq/cell;[41,42] therefore, a 170 pL droplet containing a single cell has a radioactivity concentration of ∼29 MBq/mL. Assuming that DHRh 123 is equally sensitive in bulk solutions and in droplets and neglecting differences in the respective detection methods (plate reader versus microscope camera), we calculated the theoretical intensity ratio between empty droplets and those encapsulating a radiolabeled single cell. Given these assumptions, we determined that a droplet with a single cell emits a signal that is 4.2-fold more intense than an empty droplet. This result points toward the feasibility of the intended approach by DHRh 123 activation; however, the influence of different detection platforms with dissimilar efficiencies needs to be evaluated experimentally.

Fluorescence Activation of Radiofluorogenic Droplets. The dosimetric response of DHRh 123 (200 μM) in microfluidic droplets was measured by fluorescence microscopy. Empty droplets were anchored to the imaging chamber (Figure 3a) and imaged multiple times after consecutive X-ray

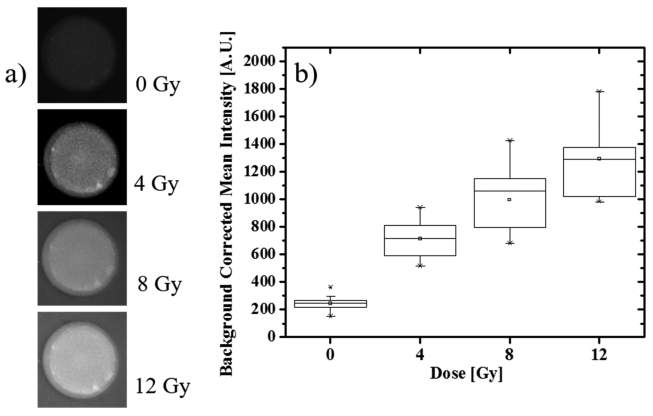

Figure 3. (a) Micrograph showing fluorescence increase of an anchored droplet containing DHRh 123 (200 μM) as a function of X-ray dose; the diameter of the anchor is 100 μm. All images were captured using the same imaging parameters (70% illumination intensity, exposure time = 500 ms). Note that the background brightness increases as a function of the dose because of DHRh 123 fractional partitioning to the oil phase. (b) Box plot of mean fluorescence intensity in anchored droplets (N = 18) exposed to different X-ray doses.

DOI: 10.1021/acs.analchem.7b00414
Anal. Chem. 2017, 89, 6472−6481

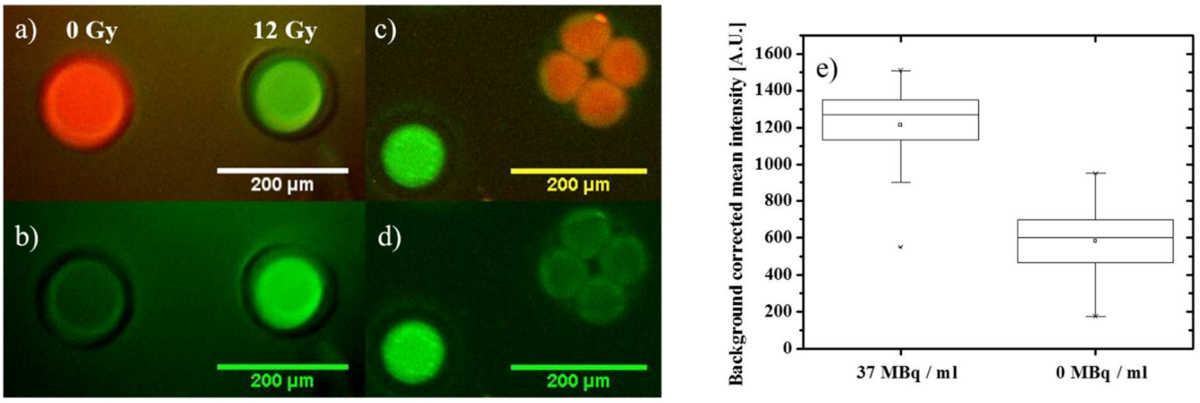

Figure 4. (a, b) Fluorescence microscopy images representing two PBS droplets containing DHRh 123 (200 μM). Unirradiated droplets were labeled with Alexa 594 (left droplet) whereas droplets irradiated with X-ray (12 Gy) were not labeled (right droplet). (a) Superposition of Texas Red (fluorescence emission from Alexa 594) and Green Fluorescence Protein (fluorescence emission from activated DHRh 123) channels, (b) Green Fluorescence Protein channel only. (c, d) Fluorescence microscopy images of representative droplets containing either [^{18}F]FDG (37 MBq/mL) or Alexa 594 (0 MBq/mL). (c) Superposition of Texas Red and Green Fluorescence Protein channels and (d) Green Fluorescence Protein channel only. All images were taken using the same images parameters (Green Fluorescence Protein Channel: 40% illumination intensity, exposure time = 500 ms. Texas Red Channel: 70% illumination intensity, exposure time = 750 ms). (e) Difference in mean fluorescence intensity distributions in droplets exposed to 0 MBq/mL (N = 50) and 37 MBq/mL (N = 33). Mean intensity distributions were corrected for background intensity.

exposures. Analogous to the bulk experiment, the background-corrected mean fluorescence intensity of droplets increased linearly as a function of X-ray dose (Figure 3b) ($R^2 > 0.97$). To quantify the detection limit of this new configuration, we took in consideration the ensemble of droplets present in the overall field of view (N = 18) and described the smallest significant intensity difference ΔI_R as

$$\Delta I_R > 2\sqrt{{\sigma_R}^2 + {\sigma_0}^2} \quad (4)$$

where σ_R and σ_0 correspond to the standard deviations of the intensity distributions in droplets exposed to a prescribed dose and zero dose, respectively. For a linear response (see Table S1 for details), the microscopic detection limit was determined to be 3 Gy. The worse dosimetric performance of microscopic droplet compared to bulk solutions of DHRh 123 may be attributed to a number of factors, including (1) inhomogeneous droplet size, (2) reduced accuracy and/or sensitivity of the detection system (microscope camera vs photomultiplier), (3) uneven illumination and detection efficiency within the field of view, and (4) small size of the sampling volume. In addition, we observed that rhodamine 123 (and most likely DHRh 123) can partition to the oil phase and adsorb on the PDMS wall, affecting the concentration within the droplet and the background levels. Given this issue, the potential exchange of DHRh 123 molecules between neighboring droplets through the oil phase must be investigated. For this purpose, we generated two groups of droplets from separate samples containing equal concentration of DHRh 123 (200 μM). Prior to droplet generation, one solution was exposed to X-ray (12 Gy) and the other, used for a control, was kept in the dark and mixed with a reference dye (Alexa 594). As shown in Figure 4a,b, irradiated droplets emitted a strong fluorescence signal, which was stable for over 4 h (Figure S4). In contrast, fluorescence activation remained minor in the control group during the entire time of investigation, allowing us to neglect exchange phenomena between droplets.

Given its optimal dosimetry response, this array of microdroplets may be suitable for applications other than cell measurements. For instance, several chemical dosimetry systems have been developed for measuring the characteristics of radiotherapy treatment beams,[40,43,44] but these systems do not provide spatial resolution. By encapsulating a chemical dosimeter such as DHRh 123 in an array of droplets, it is possible to make spatial measurements using a chemical dosimeter, which is not otherwise possible. The droplet system presents potential advantages over dosimetric film: first, fluorescence emission has an intrinsically lower background than optical absorption and it can be read out directly (possibly in real-time), with no need for a chemical developing procedure. Furthermore, the radiofluorogenic droplets demonstrate a highly linear response to ionizing radiation dose, and the arrayed droplets may deliver accurate quantifications of the radiation dose with spatial resolution on the order of 100 μm. Since spatial resolution is primarily determined by the droplet size and the interdroplet distance, the platform can be customized for a broad range of applications requiring different resolution requirements.

Fluorescence activation of radiofluorogenic droplets by radiopharmaceuticals was also evaluated by mixing DHRh 123 with either [^{18}F]FDG (37 MBq/mL) or with the reference dye Alexa 594, used as a control. In these experiments, the mixing step was performed immediately before generating the droplets to make sure that fluorescence activation would occur exclusively within microdroplets. Figure 4c,d shows the strong fluorescence activation of droplets containing [^{18}F]FDG in comparison with the control group. The difference in fluorescence intensity between radioactive and nonradioactive (control) droplets persisted over 4 h. Furthermore, cross-contamination between neighboring droplets was negligible, even when radioactive and nonradioactive droplets were trapped in the same anchor (Figure S5). Fluorescence activation was quantified by measuring the distribution of fluorescence intensity over control (N = 50) and radioactive (N = 33) droplets (Figure 4e). On average, radiolabeled droplets were about 2-fold brighter. This difference can be enhanced further by optimizing the acquisition parameters, such as the intensity of the light source and the exposure time. In addition, intensity distributions can be significantly narrowed by selecting a smaller region of interest in the field of view.

DOI: 10.1021/acs.analchem.7b00414
Anal. Chem. 2017, 89, 6472−6481

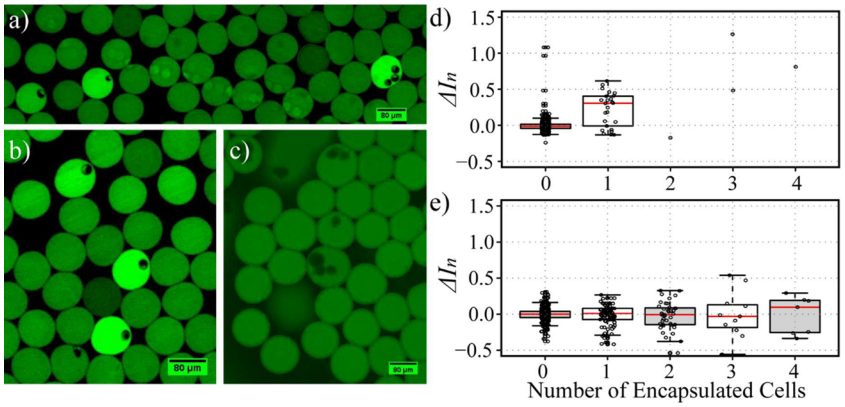

Figure 5. Fluorescence activation by radionuclide uptake in single cells. (a and b) Fluorescence microscopy images (FITC channel) of droplets loaded with cells that had previously been incubated with [^{18}F]FDG. (c) Same as previous, for cells not incubated with a radiotracer. (d) Distribution of relative fluorescence intensity as a function of cell number occupancy (n) in droplets containing radiolabeled cells. The difference between empty (n = 0) and occupied (n = 1) droplets is statistically significant ($P < 10^{-4}$ for α = 0.05). (e) Same as previous, for control cells. The difference between empty and occupied droplets is not statistically significant (for n = 1, 2, 3; P = 0.807, 0.980, 0.222, respectively, for α = 0.05). Images a and b were collected using 50% illumination intensity, exposure time = 146 ms, and gain = 1.02, while image c was collected using 90% illumination, exposure time 11 ms, and gain = 3.11.

Radiofluorogenic Droplets As Cellular Assay. The fluorescence activation of radiofluorogenic droplets containing radiolabeled human MDA-MB-231 breast cancer cells was investigated. Cells were labeled with [^{18}F]FDG (37 MBq/mL) and with a nuclear counterstain to facilitate identification and counting. Although [^{18}F]FDG radioactivity is known to damage DNA, this effect is reversible and cell viability, trans-differentiation, and functions are not significantly impacted.[41] Once suspended in PBS, cells were flowed into the microfluidic channel and mixed with DHRh 123 (400 μM) at the inlet, immediately before droplet formation. The resulting droplets were collected at the outlet of the chip in a tube and, after waiting for a sufficient amount of time, they were pipetted between two coverslips to increase the number of observable droplets. Compared with imaging droplets trapped in the anchors, this procedure increased the imaging throughput, making it possible to observe tens of droplets with single-cell occupancy in a single experiment. Figure 5a,b shows two representative fluorescence images of droplets containing one and three radiolabeled cells. The presence of radiolabeled cells caused visible fluorescence activation well above background levels. In addition, radiation contamination, i.e., unwanted fluorescence activation due to adjacent radioactive droplets, was not observed in this configuration. This may be because droplets are not static during radioactive exposure, and therefore they do not remain adjacent long enough for a pattern of contamination to appear. Empty ROS sensor droplets were used as the reference signal to normalize the fluorescence of activated droplets.

In order to quantify the extent of fluorescence activation, we described cell occupancy (n) as the number of cells present in a droplet, and we defined the relative difference in fluorescence intensity between droplets loaded with a specific number of cells n and empty droplets (n = 0) as

$$\Delta I_n = \frac{I_n - \langle I_0 \rangle}{\langle I_0 \rangle} \tag{5}$$

where $\langle I_0 \rangle$ represents the average intensity of empty droplets. The corresponding distributions are reported in Figure 5d. The relative difference ΔI_n was found statistically significant for n = 1 ($P < 10^{-4}$ at α = 0.05), while the broad distribution of the single-cell population is consistent with the well-known heterogeneity of [^{18}F]FDG uptake at the single-cell level.[15] Analogously, at higher cell occupancies, we did not find a linear correlation between n and ΔI_n. While the number of droplets containing multiple cells was too low for robust statistical analysis, the general trend suggests that ΔI_n increases with n (Figure 5d).

To rule out the possibility that the fluorescence activation is unrelated to the presence of the radiotracer, a control experiment was performed under similar conditions with nonradioactive cells (Figure 5c). In this case, all droplets presented similar fluorescence intensities, independently of cell occupancy (Figure 5e). From a statistical point of view, the relative difference between empty droplets and droplets containing one or more cells was not significant (for n = 1,2,3, P = 0.807, 0.980, 0.222, respectively, for α = 0.05), indicating that fluorescence activation is due to the radiotracer present in the cells and not to long-lived cellular ROS. In addition, consistently with the interpretation attributing the broad distribution in fluorescence activation to the heterogeneity in the single-cell uptake of [^{18}F]FDG, in the absence of the radiotracer, such distribution was found to be considerably narrower (see Figure 5e).

In summary, results from the control experiment confirm that fluorescence activation is due to radioactive decay of [^{18}F]-FDG, proving the potential of this novel approach. This is the first time, to our knowledge, that the cellular uptake of radiolabeled molecules is revealed through the activation of radiofluorogenic droplets. In future experiments, the sensitivity of the detection method will be improved by the use of more precise syringe pumps for generating droplets, and non-PDMS-based microfluidic technology will be applied to avoid the adsorption of the sensor into the walls of the microchannel. Current studies are also focused on the development of nanoparticle-based ROS sensors[45] specifically designed for this application, to use in place of commercial indicators. In the future, we will also investigate the possibility of introducing free radical promoters such as titanocene into the droplets[46] to enhance the response of ROS sensors to ionizing radiation.

DOI: 10.1021/acs.analchem.7b00414
Anal. Chem. 2017, 89, 6472−6481

CONCLUSION

In this work, we presented a new method for the detection of radiolabeled small molecules in single cells through the permanent activation of radiofluorogenic droplets. By converting radioactive decays into a permanent fluorescence signal, this approach avoids the need for long acquisitions since, contrary to radioactivity, fluorescence can be measured rapidly with high throughput. The principal component of this assay is the ROS sensor, i.e., a molecular probe which produces a fluorescence signal as an indirect response to ionizing radiation, mediated by water radiolysis.

To establish the optimal working conditions, the radiation response of seven commercial sensors was examined in bulk solutions. DHRh 123 was selected as the lead candidate given its favorable linearity, sensitivity, brightness, and stability. Fluorescence intensity of DHRh 123 in bulk increased 54% per Gy following X-ray irradiation, and 15% per MBq/mL following incubation with [^{18}F]FDG for after 3.4 h. However, this investigation also highlighted the limitations of available commercial probes, which were shown to spontaneously activate over time, giving rise to fluorescence signals even in the absence of ionizing radiation.

These experiments were repeated in droplets under similar conditions. The fluorescence intensity of individual droplets was found to increase linearly with X-ray dose and radiotracer concentration. Cross-contamination between adjacent droplets was not observed in experiments and computer simulations confirmed that any physical contamination would be well under the experimental measurement error. Through these experiments, the droplet sensor was found to be less sensitive than the bulk sensor, with a physical detection limit of 3 Gy per droplet. This finding is attributed primarily to droplet-to-droplet variability but also to the lower sensitivity of the microscope (compared to the PMT-based microplate reader) and to the instability of the sensor, which tends to partition to the oil phase and adsorb into PDMS.

Finally, radiolabeled cells were encapsulated in DHRh 123 droplets to validate the assay in living cells. Unambiguous activation was visualized for droplets containing one or more radiolabeled cells, while negligible activation was observed in droplets containing nonradiolabeled cells. Our findings constitute the first demonstration that the uptake of radiotracers in single cells can be detected by fluorescence activation in microdroplets. This novel approach paves the way for the introduction of fluorescence-based methods to quantify the uptake of radioactive small molecules in single cells, with possible applications ranging from analytical assays for cancer and other diseases to the development of small-molecule drugs. In future studies, we aim to increase the sensitivity of the assay by 1 order of magnitude to enable the quantification of radioactivity in single cells. This could be achieved by improving the formulation of the sensor, the uniformity and size of the droplets, and the readout method. For instance, Monte Carlo simulations have shown that higher ROS concentrations can be achieved with smaller droplets. Nanoparticle-based ROS sensors could also be used for greater sensitivity and stability.

In conclusion, this droplet-based radiometric assay is a promising approach for studying the heterogeneous biophysical properties of single cells using radionuclide probes. Small radiofluorogenic droplets are ideally suited for measuring the radioactivity of single cells. In addition, they could even be used for precise microdosimetry of radiation therapy beams. In our vision, specific sorting of subpopulations of cells could be performed downstream using microfluidic devices. In this framework, the integration of optical methods with cellular targeting by radioactive tracers opens the way for analyzing molecular and metabolic processes with molecular specificity and high throughput. In addition, radionuclide substitution will allow for more accurate studies of the biochemical activity of specific small molecules, whereas functionalization with organic fluorophores is likely to significantly impact the chemical structure.

ASSOCIATED CONTENT

Supporting Information

The Supporting Information is available free of charge on the ACS Publications website at DOI: 10.1021/acs.analchem.7b00414.

Dosimetric response of single sensor droplets exposed to X-ray, Monte Carlo simulations, radiation response of various ROS sensors, and influence of sensor concentration, increase in fluorescence intensity in droplets over time, and fluorescence microscopy images of mixed populations of droplets (PDF)

AUTHOR INFORMATION

Corresponding Author

*Phone: +1 650 724 9829. Fax: +1 650 723 7254. E-mail: pratx@stanford.edu.

ORCID

Maria Elena Gallina: 0000-0002-3949-5536

Author Contributions

×M.E.G. and T.J.K. contributed equally to the work.

Notes

The authors declare no competing financial interest.

ACKNOWLEDGMENTS

The authors gratefully acknowledge Ian Smeenk for the fabrication of some of the molds and microfluidic chips, the Stanford Cyclotron Radiochemistry Facility staff (Bin Shen, George Montoya, and Shawn Scatliffe) for producing/packing [^{18}F]FDG and Stanford Environmental Health and Safety (LeAnne Amoroso and Doug Menke) for delivering [^{18}F]FDG. This work was supported by the National Institutes of Health [Grant NIH NCI 1R21CA193001] and a Stanford ChEM-H seed grant; Guillem Pratx is a Damon Runyon-Rachleff Innovator supported (in part) by the Damon Runyon Cancer Research Foundation (DRR-36-15); Tae Jin Kim is supported in part by NCI Training Grant T32 CA118681.

REFERENCES

(1) Lin, C.; Bradshaw, T. J.; Perk, T. G.; Harmon, S.; Eickhoff, J.; Jallow, N.; Choyke, P.; Dahut, W.; Larson, S. M.; Humm, J. L.; Perlman, S.; Apolo, A. B.; Morris, M. J.; Liu, G. X.; Jeraj, R. *J. Nucl. Med.* **2016**, *57*, 1872.

(2) Cherry, S. R. *J. Nucl. Med.* **2006**, *47*, 1735−1745.

(3) Gambhir, S. S. *Nat. Rev. Cancer* **2002**, *2*, 683−693.

(4) Massoud, T. F. *Genes Dev.* **2003**, *17*, 545−580.

(5) Surasi, D. S.; Bhambhvani, P.; Baldwin, J. A.; Almodovar, S. E.; O'Malley, J. P. *J. Nucl. Med. Technol.* **2014**, *42*, 5−13.

(6) Liu, Z.; Jian, Z.; Wang, Q.; Cheng, T.; Feuerecker, B.; Schwaiger, M.; Huang, S.-C.; Ziegler, S. I.; Shi, K. *J. Nucl. Med.* **2016**, *57*, 1548−1555.

DOI: 10.1021/acs.analchem.7b00414
Anal. Chem. 2017, 89, 6472−6481

(7) Brooks, M. D.; Burness, M. L.; Wicha, M. S. *Cell Stem Cell* **2015**, *17*, 260−271.
(8) Tang, D. G. *Cell Res.* **2012**, *22*, 457−472.
(9) Shackleton, M.; Quintana, E.; Fearon, E. R.; Morrison, S. J. *Cell* **2009**, *138*, 822−829.
(10) Barlogie, B.; Raber, M. N.; Schumann, J.; Johnson, T. S.; Drewinko, B.; Swartzendruber, D. E.; Göhde, W.; Andreeff, M.; Freireich, E. J. *Cancer Res.* **1983**, *43*, 3982−3997.
(11) Yeo, T.; Tan, S. J.; Lim, C. L.; Lau, D. P. X.; Chua, Y. W.; Krisna, S. S.; Iyer, G.; Tan, G. S.; Lim, T. K. H.; Tan, D. S. W.; Lim, W.-T.; Lim, C. T. *Sci. Rep.* **2016**, *6*, 22076.
(12) Xue, M.; Wei, W.; Su, Y.; Kim, J.; Shin, Y. S.; Mai, W. X.; Nathanson, D. A.; Heath, J. R. *J. Am. Chem. Soc.* **2015**, *137*, 4066−4069.
(13) Pratx, G.; Chen, K.; Sun, C.; Axente, M.; Sasportas, L.; Carpenter, C.; Xing, L. *J. Nucl. Med.* **2013**, *54*, 1841−1846.
(14) Natarajan, A.; Türkcan, S.; Gambhir, S. S.; Pratx, G. *Mol. Pharmaceutics* **2015**, *12*, 4554−4560.
(15) Pratx, G.; Chen, K.; Sun, C.; Martin, L.; Carpenter, C. M.; Olcott, P. D.; Xing, L. *PLoS One* **2012**, *7*, e46285.
(16) Kim, T. J.; Tuerkcan, S.; Ceballos, A.; Pratx, G. *Biomed. Opt. Express* **2015**, *6* (11), 4585.
(17) Sengupta, D.; Miller, S.; Marton, Z.; Chin, F.; Nagarkar, V.; Pratx, G. *Adv. Healthcare Mater.* **2015**, *4*, 2064−2070.
(18) Phelps, M. E. *J. Nucl. Med.* **2000**, *41*, 661−681.
(19) Cairns, R. A.; Harris, I. S.; Mak, T. W. *Nat. Rev. Cancer* **2011**, *11*, 85−95.
(20) Sengupta, D.; Pratx, G. *J. Nucl. Med.* **2016**, *57*, 1136−1140.
(21) Warman, J. M.; de Haas, M. P.; Luthjens, L. H.; Murrer, L. H. P. *Adv. Mater.* **2011**, *23*, 4953−4955.
(22) Warman, J. M.; de Haas, M. P.; Luthjens, L. H. *Phys. Med. Biol.* **2009**, *54*, 3185−3200.
(23) Boudou, C.; Troprès, I.; Rousseau, J.; Lamalle, L.; Adam, J. F.; Estève, F.; Elleaume, H. *Phys. Med. Biol.* **2007**, *52*, 4881−4892.
(24) Yukihara, E. G.; McKeever, S. W. S. *Phys. Med. Biol.* **2008**, *53*, R351−R379.
(25) Niroomand-Rad, A.; Blackwell, C. R.; Coursey, B. M.; Gall, K. P.; Galvin, J. M.; McLaughlin, W. L.; Meigooni, A. S.; Nath, R.; Rodgers, J. E.; Soares, C. G. *Med. Phys.* **1998**, *25*, 2093−2115.
(26) Soares, C. G. *Radiat. Prot. Dosim.* **2006**, *120*, 100−106.
(27) Gomes, A.; Fernandes, E.; Lima, J. L. F. C. *J. Biochem. Biophys. Methods* **2005**, *65*, 45−80.
(28) Sandwall, P. A.; Spitz, H. B.; Elson, H. R.; Lamba, M. A. S.; Connick, W. B.; Fenichel, H. *J. Radioanal. Nucl. Chem.* **2016**, *307*, 2505−2508.
(29) Türkcan, S.; Nguyen, J.; Vilalta, M.; Shen, B.; Chin, F. T.; Pratx, G.; Abbyad, P. *Anal. Chem.* **2015**, *87*, 6667−6673.
(30) Wang, H.; Joseph, J. A. *Free Radical Biol. Med.* **1999**, *27*, 612−616.
(31) Richardson, M. P.; Ayliffe, M. J.; Helbert, M.; Davies, E. G. *J. Immunol. Methods* **1998**, *219*, 187−193.
(32) Pap, E. H. W.; Drummen, G. P. C.; Winter, V. J.; Kooij, T. W. A.; Rijken, P.; Wirtz, K. W. A.; Op den Kamp, J. A. F.; Hage, W. J.; Post, J. A. *FEBS Lett.* **1999**, *453*, 278−282.
(33) Mazutis, L.; Gilbert, J.; Ung, W. L.; Weitz, D. A.; Griffiths, A. D.; Heyman, J. A. *Nat. Protoc.* **2013**, *8*, 870−891.
(34) Baret, J.-C.; Miller, O. J.; Taly, V.; Ryckelynck, M.; El-Harrak, A.; Frenz, L.; Rick, C.; Samuels, M. L.; Hutchison, J. B.; Agresti, J. J.; Link, D. R.; Weitz, D. A.; Griffiths, A. D. *Lab Chip* **2009**, *9*, 1850.
(35) Stephan, K.; Pittet, P.; Renaud, L.; Kleimann, P.; Morin, P.; Ouaini, N.; Ferrigno, R. *J. Micromech. Microeng.* **2007**, *17*, N69−N74.
(36) Anna, S. L.; Bontoux, N.; Stone, H. A. *Appl. Phys. Lett.* **2003**, *82*, 364.
(37) Abbyad, P.; Dangla, R.; Alexandrou, A.; Baroud, C. N. *Lab Chip* **2011**, *11*, 813−821.
(38) Schwarz, H. A. *J. Chem. Educ.* **1981**, *58*, 101.
(39) Kundu, K.; Knight, S. F.; Willett, N.; Lee, S.; Taylor, W. R.; Murthy, N. *Angew. Chem., Int. Ed.* **2009**, *48*, 299−303.
(40) Ashawa, S. C.; Kini, U. R.; Madhvanath, U. *Int. J. Appl. Radiat. Isot.* **1979**, *30*, 7−10.
(41) Elhami, E.; Goertzen, A. L.; Xiang, B.; Deng, J.; Stillwell, C.; Mzengeza, S.; Arora, R. C.; Freed, D.; Tian, G. *Eur. J. Nucl. Med. Mol. Imaging* **2011**, *38*, 1323−1334.
(42) Zhang, Y.; DaSilva, J. N.; Hadizad, T.; Thorn, S.; Kuraitis, D.; Renaud, J. M.; Ahmadi, A.; Kordos, M.; deKemp, R. A.; Beanlands, R. S.; Suuronen, E. J.; Ruel, M. *Cell Transplant.* **2012**, *21*, 1821−1835.
(43) Collins, A. K.; Makrigiorgos, G. M.; Svensson, G. K. *Med. Phys.* **1994**, *21*, 1741−1747.
(44) Barreto, J. C.; Smith, G. S.; Strobel, N. H. P.; McQuillin, P. A.; Miller, T. A. *Life Sci.* **1994**, *56*, PL89−PL96.
(45) Shuhendler, A. J.; Pu, K.; Cui, L.; Uetrecht, J. P.; Rao, J. *Nat. Biotechnol.* **2014**, *32*, 373−380.
(46) Kotagiri, N.; Sudlow, G. P.; Akers, W. J.; Achilefu, S. *Nat. Nanotechnol.* **2015**, *10*, 370−379.

DOI: 10.1021/acs.analchem.7b00414
Anal. Chem. 2017, 89, 6472−6481